Rapid and Label-Free Single-Nucleotide Discrimination *via* an Integrative Nanoparticle–Nanopore Approach

Yan Shan Ang and Lin-Yue Lanry Yung*

Department of Chemical and Biomolecular Engineering, National University of Singapore, 10 Kent Ridge Crescent, Singapore 119260, Singapore

ABSTRACT

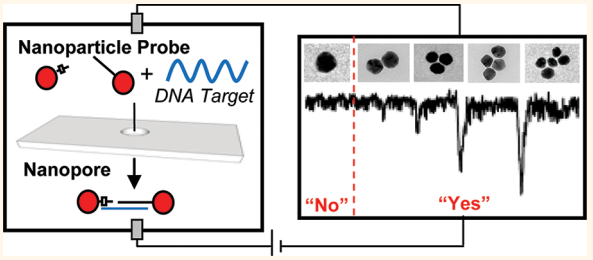

Single-nucleotide polymorphism (SNP) is an important biomarker for disease diagnosis, treatment monitoring, and development of personalized medicine. Recent works focused primarily on ultrasensitive detection, while the need for rapid and label-free single-nucleotide discrimination techniques, which are crucial criteria for translation into clinical applications, remains relatively unexplored. In this work, we developed a novel SNP detection assay that integrates two complementary nanotechnology systems, namely, a highly selective nanoparticle–DNA detection system and a single-particle sensitive nanopore readout platform, for rapid detection of single-site mutations. Discrete nanoparticle–DNA structures formed in the presence of perfectly matched (PM) or single-mismatched (SM) targets exhibited distinct size differences, which were resolved on a size-tunable nanopore platform to generate corresponding "yes/no" readout signals. Leveraging the *in situ* reaction monitoring capability of the nanopore platform, we demonstrated that real-time single-nucleotide discrimination of a model G487A mutation, responsible for glucose-6-phosphate dehydrogenase deficiency, can be achieved within 30 min with no false positives. Semiquantification of DNA samples down to picomolar concentration was carried out using a simple parameter of particle count without the need for sample labeling or signal amplification. The unique combination of nanoparticle-based detection and nanopore readout presented in this work brings forth a rapid, specific, yet simple biosensing strategy that can potentially be developed for point-of-care application.

KEYWORDS: nanopore · gold nanoparticle · nanoparticle assembly · single-nucleotide polymorphism · real-time detection · label-free

Single-nucleotide polymorphism (SNP) refers to the difference of one nucleotide in the genome, which accounts for about 90% of all genetic variations and occurs approximately every 100 to 300 bases.[1] Due to its prevalence in the population, SNP represents an important biomarker of clinical significance in medical diagnostics.[2] There is therefore a demand for developing a detection system capable of picking up this subtle single-nucleotide difference to achieve early disease detection, monitor response to treatment, and allow better prognosis.[3]

Currently, the common detection techniques are real-time polymerase chain reaction (RT-PCR) and microarray. The former lacks specificity in spite of tedious optimization work.[4,5] The latter allows for high-throughput DNA screening; however, stringent wash steps and precise temperature control are required for single-nucleotide discrimination. Still, occurrence of false positive results is still high, and long hybridization time is required due to inherent diffusion-limited kinetics.[6] Many have thus looked toward nanoparticle-based detection for improved sensitivity and selectivity, and ideally low cost. The use of gold nanoparticles (nAu) received much attention due to their numerous unique physical and chemical properties, rendering them an ideal biosensing candidate.[7] In particular, nAu functionalized with DNA strands (nAu-DNA)[8,9] has been used extensively to probe for specific DNA sequences in various formats.[10–13] Due to the sharp melting temperature transition of nAu-DNA probes, a high selectivity of single-nucleotide discrimination can be achieved.[14]

For the purpose of diagnostics, it is essential that a precise number of DNA strands per nAu is controlled to better quantify the amount of target molecules.[15] Our group previously reported the design of a nAu-DNA probe bearing a distinct number of DNA strands to discriminate single-nucleotide mutations.[16] Two sets of non-complementary probes, one functionalized with 18b ssDNA (nAu-18b) and the other with 100b ssDNA (nAu-100b), are used. In the presence of a perfectly matched (PM) target, the two probes are linked together *via* hybridization of target DNA and form a well-defined nAu-DNA assembly (termed

* Address correspondence to cheyly@nus.edu.sg.

Received for review June 14, 2012 and accepted August 31, 2012.

Published online September 20, 2012
10.1021/nn302636z

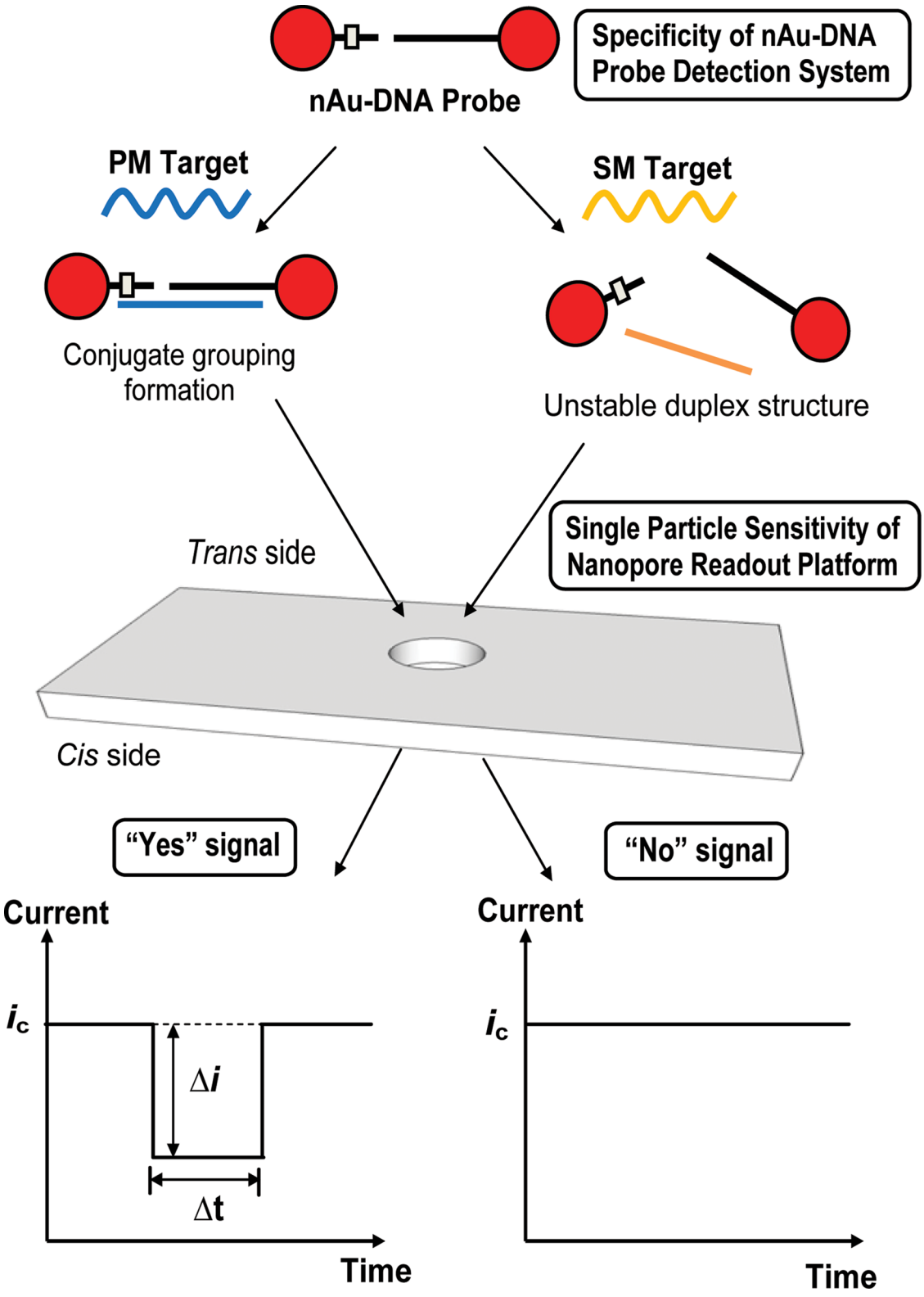

Scheme 1. Schematic illustration of nanopore-based single-nucleotide detection using a nAu-DNA probe. The ssDNA sequences on nAu-100b and nAu-18b probes were designed to be complementary to the mutant (mut) sequence and single mismatched to the wild-type (wt) sequence. In the presence of a perfectly matched (PM) target, a well-defined nanoparticle assembly, termed conjugate grouping, forms. Each distinct conjugate grouping is picked up as an individual signal ("Yes" signal) when it translocates the pore of the membrane from the *trans* to the *cis* side. Every successful translocation activity is termed a blockade event, which is characterized by its blockade magnitude (Δi) and baseline translocation duration (Δt). When a single-mismatched (SM) target is added, the intermediate duplex structure is energetically unstable and fails to form an assembly structure. The smaller-sized nAu-DNA probe does not result in an appreciable dip in baseline current (i_c) and is taken to produce a "No" signal.

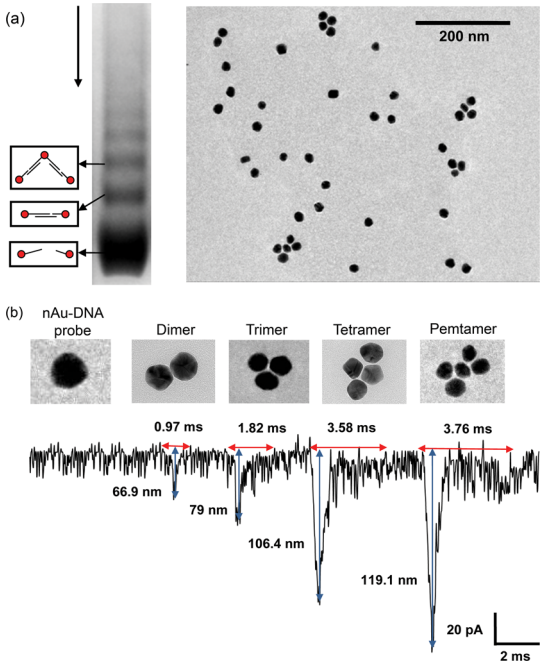

Figure 1. (a) (Left) Gel electrophoresis image of the conjugate groupings separated according to the order of assembly formed. Higher order conjugate groupings, which are larger in size, were retarded to a greater extent by the gel matrix and so migrated through a shorter distance. The direction of migration is indicated with an arrow. A representative illustration of dimeric and trimeric conjugate groupings is drawn next to the corresponding gel band and indicated with an arrow. Other unlabeled gel bands correspond to the higher order conjugate groupings (tetrameric, pentameric, *etc.*). (Right) TEM image of the hybridized mixture when 1.0 pmol of PM target was added to 5 nM nAu-100b probe and 15 nM nAu-18b probe in a 30 μL reaction volume. Discrete conjugate groupings can be directly visualized, *i.e.*, a dimer comprising two nAu-DNA probes, a trimer comprising three nAu-DNA probes, and so on. (b) Raw signal trace of the respective order of conjugate groupings. A representative trace of an individual blockade event, obtained from separate experiments, was truncated for each order and spliced together to form a continuous readout signal for illustration purposes. The mean baseline blockade duration and modal blockade magnitude of each population are indicated using red and blue arrows, respectively, with the corresponding values stated.

conjugate grouping) (Scheme 1). When a single-mismatched (SM) target is added, the duplex structure is energetically unstable and no conjugate grouping forms. Previously, gel electrophoresis was used as a readout platform to visualize single-nucleotide mismatch with our nAu-DNA probes.[17] Despite its ease of use, rapid detection is lacking. This has prompted our search for an alternative readout platform to complement our highly specific nAu-DNA detection system.

A nanopore platform is a suitable candidate as its single-molecule/particle sensitivity facilitates the rapid picking up of signal from our discrete conjugate groupings. Its simplicity of design and operation as well as label-free characteristics is a continuation of the ease of use associated with gel platforms. The fundamental concept of nanopore technology is based on Coulter counting or resistive pulse sensing principle.[18] Two fluid chambers filled with electrolyte buffer are separated by a membrane, and the nanoscopic pore opening is the only passage for ions or particles to flow through (Scheme S1). Under the influence of an electric field, particles translocate through the pore singly, leading to a dip in ionic current flowing through the pore. Each translocation activity is termed a blockade event, with the corresponding drop in baseline current (blockade magnitude, Δi) and the time of translocation (baseline translocation duration, Δt) reflecting particle size and charge, respectively. The ratio of Δi to baseline current (i_c) is approximately the same as the ratio of particle volume to pore volume for a cylindrical pore based on the following equation:[19]

$$\frac{\Delta i}{i_c} = S(d_c, d_s)\frac{{d_s}^3}{(l_c + 0.785d_c){d_c}^2} \quad (1)$$

where d_s is the particle diameter, d_c is the pore diameter, and l_c is the pore length. $S(d_c,d_s)$ is the correction factor dependent on the diameter ratio, d_c/d_s.

Since the resurgence of interest in the use of nanopores for DNA sequencing,[20] various groups have extended the use of this tool for other applications, such as detection of viruses[21] and nucleic acid,[22] as well as characterization of nanoparticle size and surface charge.[23] Its real-time *in situ* reaction monitoring capability has provided insights into fundamental mechanisms of protein−protein interaction,[24] antibody−antigen binding,[25] and single-molecule transport across a nuclear pore complex.[26] One recent nanopore-based microRNA (miRNA) expression profiling work reported by Wanunu *et al.* demonstrated the ability of the nanopore to not only detect a specific miRNA sequence but also accurately quantify the miRNA amount down to the subfemtomole level.[27] An additional advantage of using nanopore-based detection is that the measurement error can be lowered when more time is allowed for data recording. This highlights the potential of having nanopores as a rapid yet accurate sensing platform.

Herein, we propose the use of a novel nanopore readout platform to pick up individual distinct signals from our well-defined nAu-DNA conjugate groupings *in situ* as the nAu-DNA probes hybridize with the PM target DNA for rapid single-nucleotide discrimination (Scheme 1). The proportionality relationship in eq 1 is approximately true for conical pores. Using an elastic conical-shaped polyurethane membrane, the pore size can be tuned such that Δi is of significant value only for larger-sized conjugate groupings formed in the presence of a PM target, while a negligible signal is obtained for the SM target. In addition to the single-particle sensitivity offered by nanopore detection, our proposed scheme has the advantages of shorter analysis time and simplified detection and readout steps in a single workflow procedure.

RESULTS AND DISCUSSION

Characterization of a nAu-DNA Conjugate Grouping. The direct method of DNA sequencing *via* the nanopore platform suffers from high translocating velocity, rendering it challenging to pick up signals accurately from each nucleotide, much less differentiating the subtle electronic difference for single-nucleotide discrimination.[28] Our nAu-DNA probe system can slow the translocation speed significantly for clear, distinct signals to be picked up. Moreover, there is an obvious size difference between nAu-DNA probes and conjugate groupings as seen from their differences in electrophoretic mobility and the TEM image in Figure 1a. In this study, our nAu-DNA probes were designed to detect the G487A mutation, a major genetic variant responsible for glucose-6-phosphate dehydrogenase (G6PD) deficiency.[29] Larger sized conjugate groupings formed only in the presence of the mutant strand to which our probes were perfectly matched, while smaller sized nAu probes signified the presence of wild-type or, otherwise, single-mismatched target DNA. By making use of such a distinct size disparity, differences in electronic signals for PM and SM targets can be magnified significantly since the blockade signals are directly proportional to the particle volume.

The clarity in readout signals was further augmented *via* the use of a tunable membrane that can be stretched to a sufficiently large pore size such that the nAu-DNA probe-to-pore volume ratio resulted in a negligible readout signal. The feasibility of this strategy was demonstrated in Figure 1b, in which the smaller sized nAu-DNA probe was drowned in the electronic noise and appreciable blockade events were registered only for dimers and higher order conjugate groupings. The observed trend of increasing diameter and baseline blockade duration for higher order conjugate groupings is in line with theoretical expectation since larger sized conjugate groupings give rise to a larger dip in baseline current and encounter greater impedance to their movement through the pore. This strongly indicated that the positive signals obtained were indeed contributed by the conjugate groupings population. A similar strategy of using a unique probe design to generate signature signals was previously reported.[30] In their design, a multilevel current pattern had to be identified for signal differentiation, which can complicate data interpretation considerably. Our probe design offers a more straightforward "yes"/"no" readout to indicate the presence or absence of the interrogated target.

Though the modal diameter value was close to the expected value of each conjugate grouping order, *i.e.*, 50 nm for dimer, 75 nm for trimer, 100 nm for tetramer, and 125 nm for pentamer, distinct signature signals could not be characterized due to the wide size distribution involved (Figure S1). Since our conjugate groupings are nonspherical, there could be differences

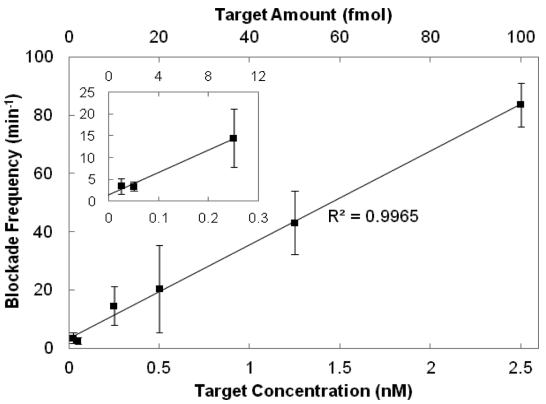

Figure 2. Standard calibration curve relating blockade frequency (min^{-1}) to target concentration (nM). Results are mean ± SD. The mean was obtained by averaging the values of 10 sample points collected at 1 min intervals over a total analysis time of 10 min. A linear correlation was obtained (R^2 = 0.9965), which can be used for semiquantification of target DNA. Inset: Blockade frequency for lower end concentration (0−0.25 nM). The blockade frequency for the control setup, *i.e.*, nAu-DNA probe with SM target added, is f_{SM} = 1.5 ± 0.7 min^{-1}. The limit of detection, defined as ±3 SD of f_{SM}, was found to be 5.0 pM or 200 amol.

in orientation and rotation of particles during translocation through the pore. This resulted in differential blockade signals despite having the same volume as predicted by the theoretical model.[31] A similar observation was made by Yusko *et al.*, whereby proteins of complex molecular shape give a broader distribution of blockade magnitude.[32] Further investigation has to be carried out to understand the fundamental mechanism involved during translocation. For the purpose of end-point detection, it is sufficient to know that positive blockade signals are indeed indicative of conjugate groupings that form only in the presence of a PM target even though there are only subtle differences between the respective orders.

Quantification of PM Target. Our nAu-18b and nAu-100b probes were designed to be noncomplementary to each other. As such, conjugate groupings formed only when linked by a PM target in a tail-to-tail configuration. Therefore, blockade frequency, which is directly related to the conjugate grouping concentration, indicates the PM target concentration. A highly linear calibration curve (R^2 = 0.9965) correlating blockade frequency to target concentration was obtained for the concentration range from 5.0 pM to 2.5 nM (Figure 2). A significant extent of variability was observed. This could be due to the clogging of the pore over time, which hampered smooth particle translocation. As such, the developed platform is suitable only for semiquantification of target DNA. Further improvement to the pore performance is required for precise quantification.

The limit of detection, defined as the PM target concentration with mean blockade frequency three standard deviations from the corresponding SM target

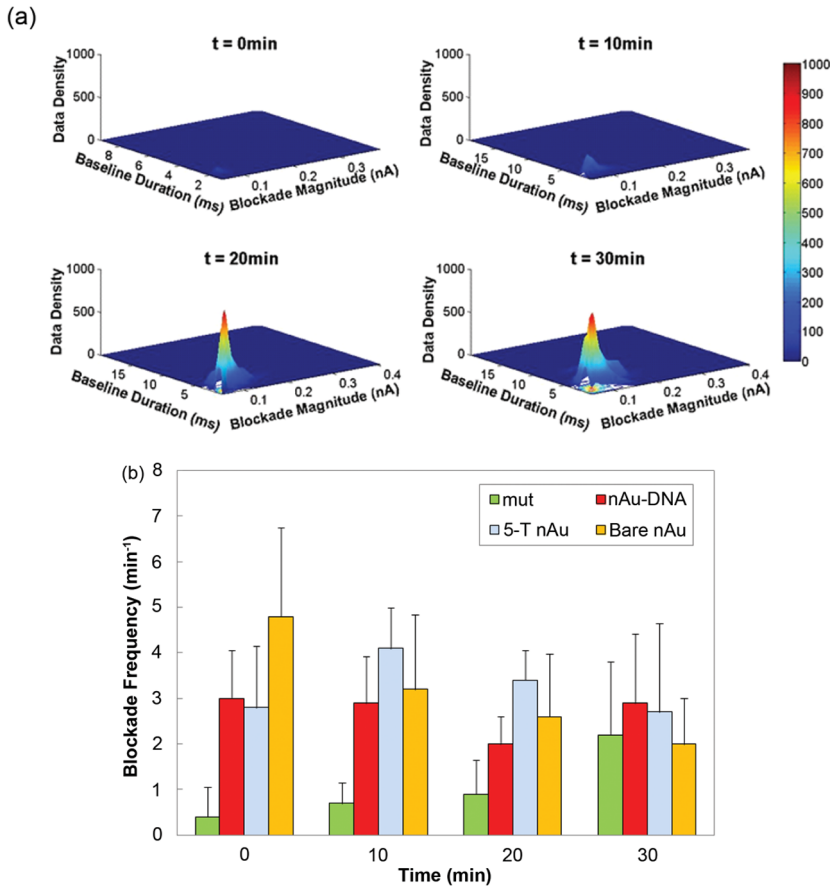

Figure 3. (a) Development of blockade events when 0.1 nM nAu-DNA probe was loaded with 1.0 pmol of PM target in a 40 μL reaction volume. Data recording was carried out from $t = 0$ min to $t = 30$ min in 10 min intervals. Appreciable growth in signal peak was observed, indicating that the initial rate of hybridization between the PM target and nAu-DNA probe was rapid enough for a detectable amount of conjugate groupings to form. (b) Blockade frequency (min^{-1}) taken at 10 min time intervals for control samples, *i.e.*, mutant strand (mut), nAu-DNA probe (nAu-DNA), nAu passivated with 5-T (5-T nAu), and unmodified nAu (bare nAu). Results shown are mean $\pm$ SD. The controls were not statistically different from one another at the 95% confidence level (two-tailed Student's *t* test). The satellite signals were likely to be inherent to the nAu population, such as larger size of the distribution, rather than due to nonspecific interaction between ssDNA and the nAu-DNA probe.

sample, was determined to be 5.0 pM or 200 amol. Though not as sensitive as other nanoparticle-based detection techniques, such as the biobarcode method (zeptomolar)[33] or scanometric assay (femtomolar),[34] it suffices for analyzing PCR-amplified DNA samples. Compared to other ultrasensitive detection, this method has the advantage of being truly label-free. Tedious labeling or signal amplification steps, such as silver enhancement, are not required, which minimizes the risks of error and enhances the simplicity and ease of use of this platform.

Feasibility of *in Situ* Conjugate Grouping Formation. Given the single-molecule sensitivity and *in situ* reaction monitoring capability of the nanopore platform, we postulate that a detectable amount of conjugate groupings can form within a short time period of target addition if the initial rate of hybridization is sufficiently rapid. To prove this hypothesis, we first investigated the conjugate grouping formation in real time on a nanopore. As before, the pore size of the membrane was mechanically actuated such that unbound nAu-DNA probes gave little to no signal, while the larger sized conjugate groupings returned positive blockade events. Blockade frequency (*f*), defined as the number of blockade events in the core data set over the time interval of analysis, was used as the basis of comparison across samples. Previously reported methods include looking for shifts in baseline blockade duration[35] and changes in FWHM duration.[36] For our simple "yes/no" detection system, the more straightforward and objective parameter of blockade frequency can be used for further quantitative analysis.

Our combined strategy of size-dependent discrimination and tunable nanopore complements each component in that a positive blockade signal arises only when a conjugate grouping forms in response to specific PM target binding, leaving little ambiguity in data interpretation. A rigorous statistical analysis was also devised in this study to minimize the contribution of nonspecific aggregates toward the positive signal counts. Each information-rich single-particle blockade event defined the unique position of a data point

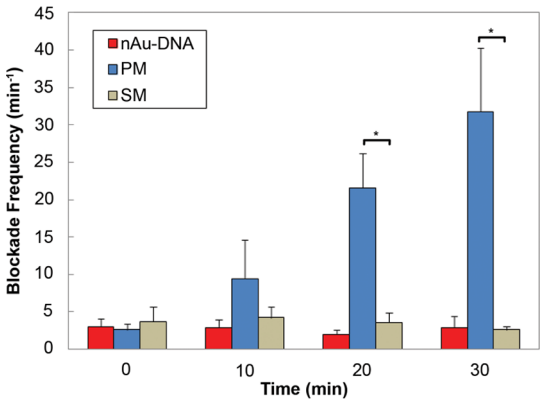

Figure 4. Blockade frequency (min^{-1}) taken at 10 min time intervals for the nAu-DNA probe control (nAu-DNA) only, probe + 1.0 pmol PM target (PM), and probe + 1.0 pmol SM target (SM). Results shown are mean ± SD. Difference in blockade frequency was statistically significant at the 20 min and 30 min mark by two-tailed Student's *t* test (*$p < 0.001$; $n = 5$).

relative to others in a scatter plot relating Δi to Δt. Blockade events outside the range of 95% of population, centered about the modal values of Δi and Δt, were considered to be outliers and excluded from further analysis (see Scheme S2 for details).

Upon loading the PM target to the *trans* side, there was a distinct growth in signal peak over time, as seen in Figure 3a. This implied that the initial rate of hybridization between nAu-DNA probes and the DNA target was sufficiently rapid. As such, the amount of conjugate groupings accumulated within the first 30 min of analysis was sufficient to be picked up by the nanopore (f_{PM} = 9.4 min^{-1} at t = 10 min, f_{PM} = 21.6 min^{-1} at t = 20 min, f_{PM} = 31.8 min^{-1} at t = 30 min). To eliminate the possibility of nonspecific binding between the nAu-18b and nAu-100b probe, a pure nAu-DNA probe as a negative control was similarly analyzed over 30 min. No appreciable increase in blockade frequency was observed ($f_{nAu\text{-}DNA}$ = 2.9 min^{-1} at t = 10 min, $f_{nAu\text{-}DNA}$ = 2.0 min^{-1} at t = 20 min, $f_{nAu\text{-}DNA}$ = 2.9 min^{-1} at t = 30 min). It was unlikely that the other component, *i.e.*, the mutant DNA strand (mut), which is much smaller in size, could have led to the increase in blockade frequency. This was confirmed by the lack of blockade signal from analyzing 1.0 pmol of mut DNA over 30 min (f_{mut} = 0.7 min^{-1} at t = 10 min, f_{mut} = 0.9 min^{-1} at t = 20 min, f_{mut} = 2.2 min^{-1} at t = 30 min), which was indistinguishable from that of pure electrolyte buffer (average f value of 0.3 min^{-1}). Therefore, hybridization of a perfectly matched DNA target with a nAu-DNA probe was the main driving force for the formation of conjugate groupings.

We noted that a nonzero blockade frequency was obtained for nAu-DNA probes. This was in excess of interference from electronic noise, which was typically lower than 0.3 min^{-1} throughout the experiments. To confirm that these satellite signals were an inherent characteristic of the nAu population, *e.g.*, larger sized

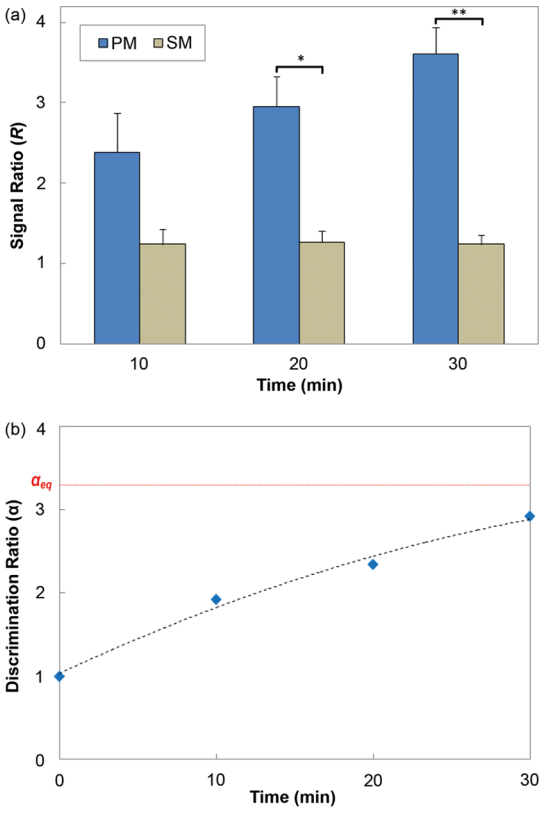

Figure 5. (a) Comparison of discriminating ability between PM and SM targets over 30 min using the signal ratio (R), defined as the ratio of blockade frequency upon target addition to that of nAu-DNA probes only. The blockade frequency at each time point is calculated by dividing the total number of filtered translocation events by the total time elapsed. Results shown are mean ± SE. Single-nucleotide discrimination was statistically significant after 20 min (95% confidence level). Two-tailed Student's *t* test was used for statistical analysis. (*$p < 0.05$, **$p < 0.005$; $n = 5$). (b) Discrimination ability of assay over time. Discrimination ratio at equilibrium (α_{eq} = 3.3) is indicated on the plot with a red, dotted line. Each data was calculated by taking the ratio of R_{PM} to R_{SM} at any time point. An α of 2.9 was already achieved by the 30 min mark. With an α_{eq} value of 3.3, 30 min was found to be satisfactory for achieving maximum assay performance, beyond which there was only marginal improvement.

particles present during synthesis or nonspecific aggregates, we performed a series of control experiments using nAu with different surface modifications. nAu passivated with 5-T ssDNA but not conjugated with a probe sequence gave comparable blockade frequency as the nAu-DNA probe ($f_{5\text{-}T}$ = 4.1 min^{-1} at t = 10 min, $f_{5\text{-}T}$ = 3.4 min^{-1} at t = 20 min, $f_{5\text{-}T}$ = 2.7 min^{-1} at t = 30 min). A similar trend was observed for unmodified bare nAu (f_{nAu} = 3.2 min^{-1} at t = 10 min, f_{nAu} = 2.6 min^{-1} at t = 20 min, f_{nAu} = 2.0 min^{-1} at t = 30 min). The results obtained for all three cases were not significantly different from one another for each time interval ($p > 0.05$) (Figure 3b). This strongly suggests that the nonspecific interaction of ssDNA on the nAu-DNA probe contributed minimally to the residual signal. Although the exact reason for the satellite signals has yet to be fully understood at this point, we have established that they

fluctuated within a narrow range, *i.e.*, 2 min^{-1} to 4 min^{-1}, which was lower than the positive signals obtained in the presence of the PM target. Hence, it suffices to treat the satellite signals as background noise inherent to the nAu population. Finally, it is worth pointing out that the blockage event signal of the nAu-DNA probe shown in Figure 1b excludes the background noise discussed here, which is not representative of the actual blockage event.

Feasibility of Real-Time Single-Nucleotide Discrimination. For successful single-nucleotide discrimination, blockade signals from the addition of a SM target should be significantly lower than that of a PM target. Our lab has previously shown that by virtue of our probe design (high surface charge from 5-T passivation), strong electrostatic repulsion forces induce a sufficient destabilizing effect such that a conjugate grouping cannot form in the presence of a single mismatch (Figure S2).[16] Another reason could be that the unstable duplex structures are disrupted as the particles migrate through the harsh gel matrix.

On the nanopore platform, a blockade frequency corresponding to addition of a SM target (f_{SM} = 4.2 min^{-1} at t = 10 min, f_{SM} = 3.6 min^{-1} at t = 20 min, f_{SM} = 2.6 min^{-1} at t = 30 min) was observed to be consistently lower than the PM target ($p < 0.001$) and cannot be distinguished from the corresponding nAu-DNA probe control ($f_{nAu\text{-}DNA}$ = 3.7 min^{-1}) (Figure 4). It could be that the strong electric field around the pore opening disrupted the formation of an unstable conjugate grouping. Since significantly different blockade signals for PM and SM targets were already obtained within 20 min, we have successfully demonstrated the feasibility of nanopore-based real-time SNP detection.

Since the total number of blockade events in the presence of the PM target was contributed by both conjugate groupings and background nAu signals, the signal-to-noise ratio was used as the basis for comparison across samples. We termed this as the signal ratio (R), which is defined as the ratio of blockade frequency upon target addition to that of nAu-DNA probes only. Within just 20 min, R corresponding to the PM target (R_{PM} = 2.96) was found to be significantly higher ($p < 0.05$) than that of the SM target (R_{SM} = 1.26) (Figure 5a). Expectedly, the signal gap between the PM and SM target widened with time. At the 30 min mark, R_{PM} increased to 3.61, while R_{SM} remained relatively constant at R_{SM} = 1.24. This is expected, as more time was allowed for the PM target to hybridize to the nAu-DNA probe, thus accumulating more conjugate groupings.

The growing signal gap was used to quantify the assay discrimination ratio (α), which is defined as the ratio of R_{PM} to R_{SM}. The discrimination ability at equilibrium was obtained by testing the same sample after 24 h of target addition. This served as a reference point to characterize the maximum assay performance. From Figure 5b, an α of 2.9 was achieved by the 30 min mark, which already started to plateau toward the equilibrium α (α_{eq}) of 3.3. A cutoff time of 30 min sufficed for rapid single-nucleotide discrimination, beyond which there was only marginal improvement in the discrimination ability of the assay. Also, no false positive was observed. Compared to our previous work involving overnight hybridization, preparation of a gel, and running the sample under gel electrophoresis, the nanopore platform has the advantages of shorter analysis time and simpler, streamlined detection-to-readout workflow. If a more sensitive and accurate detection is desired, the time of analysis can be lengthened to allow for sufficient amount of conjugate groupings to accumulate.

CONCLUSION

In this work, a novel nanopore-based assay capable of rapid single-nucleotide discrimination was developed and successfully applied for the detection of a clinically relevant point mutation. The assay involved the use of a nAu-DNA probing system to pick up specific single-site mutations in DNA targets. By tuning the pore size of the polymeric membrane, positive blockade signals were registered only for the larger sized conjugate groupings, which formed only in the presence of perfectly matched DNA targets. Leveraging the single-particle sensitivity and *in situ* reaction monitoring capability of the nanopore readout platform, we have demonstrated the feasibility for end-users to choose between rapid analysis and more sensitive detection. The real-time single-nucleotide discrimination allows a short analysis time of 30 min with no false positives. By allowing more time for hybridization of a DNA target to a nAu-DNA probe, sufficient conjugate groupings can accumulate to detect low target count. The current limit of detection is 5.0 pM of target sample, which suffices for analyzing PCR-amplified clinical samples. Semiquantification of sample concentration is possible, though further refinement is required for precise quantification. Overall, the developed assay is highly selective, rapid, and label-free with a streamlined detection and readout workflow, rendering it a promising candidate for point-of-care application.

MATERIALS AND METHODS

Materials. Hydrogen tetrachloroaurate(III) trihydrate ($HAuCl_4 \cdot 3H_2O$), trisodium citrate dihydrate ($Na_3C_6H_5O_7$), 4,4′-(phenylphosphinidene) bis(benzenesulfonic acid) dipotassium salt hydrate, and 0.1 M phosphate buffer (PB) (pH 7.5) were purchased from Sigma-Aldrich. All synthetic DNA (modified with or without a thiol linker) were purchased from Integrated DNA Technologies (IDT); 5.0 M NaCl, 0.5 M EDTA (pH 8.0), and agarose were purchased from First Base. Milli-Q water with a resistance of >18 MΩ/cm was used throughout the experiment.

Synthesis and Characterization of nAu. All glassware and magnetic stir bars were cleaned with *aqua regia* solution and rinsed thoroughly with Milli-Q water prior to use. nAu (25 nm) was synthesized by the reduction of hydrogen tetrachloroaurate(III)

trihydrate with trisodium citrate dihydrate.[37] Briefly, 4.5 mL of 1% (w/v) citrate and 45.5 mL of 0.01% (w/v) $HAuCl_4$ were preheated separately to 107 °C reaction temperature. After reaching a steady temperature for 30 min, the 1% citrate was added rapidly to the 0.01% $HAuCl_4$. After 30 min of reaction, the ripened solution was air cooled to room temperature, filtered, and stored at 4 °C until further use. A UV−vis spectrum was obtained using a Cary Varian 50 Bio UV−visible spectrophotometer. TEM characterization was carried out using a JEOL JEM-3010 transmission electron microscope operating at 300 kV. At least 100 particles were sized from TEM micrographs *via* ImageJ. A representative image is presented in Figure S3.

Fabrication of nAu-DNA Probes. Two sets of nAu-DNA probes, one 18-base ssDNA with a 3′ thiol end (nAu-18b) and the other 100-base ssDNA with a 5′ thiol end (nAu-100b), were fabricated. The ssDNA sequences are shown in Table S1. The sequences were designed to probe for G487A mutation (commonly termed Mahidol),[38] a major genetic variant responsible for G6PD deficiency.[29] Previously reported conjugation conditions[39] were used with modifications. Briefly, the molar ratio of ssDNA probe to nAu used to prepare nAu-18b and nAu-100b was 1:1 and 6:1, respectively. A modified conjugation condition of 10 mM PB (pH 7.5) and 50 mM NaCl was used. After 3 h of incubation, surface passivation was carried out using 2.0 μM 5′ SH-TTTTT 3′ ssDNA (5-T ssDNA with 5′ thiol end). The final nAu concentration was 5.0 nM in a 100 μL reaction volume. After 12 h, the salt concentration was gradually increased to 0.25 M by adding a 5.0 M NaCl solution over 6 h. The solution was incubated at room temperature for another 20 h. Unbound ssDNA was removed by repeated washing and centrifuging of the sample with 5 mM PB (pH 7.5).

Formulation of Electrolyte Buffer for Nanopore Analysis. Electrolyte buffer containing 10 mM PB (pH 7.5), 2 mM EDTA (pH 8.0), 0.01% Tween-20, and 50 mM NaCl was used for the nanopore analysis. A chelating agent, EDTA, was added to minimize aggregation due to the screening effect by divalent metal ions such as Mg^{2+}. Tween-20 confers greater stability to the nanoparticles and acts as a surfactant to promote wetting of the nanopore membrane. The mixture was vortexed for 30 s, sonicated for 2 min, and filtered using a 0.2 μm filter syringe. All prepared electrolyte buffer was stored at 4 °C until further use. The buffer was allowed to equilibrate to room temperature prior to use since the blockade signal is a function of temperature.

Nanopore Measurement and Optimization Procedure. All measurements were made using a qNano system from Izon Science. One unique property of this system is the tunable polyurethane membrane (termed qNano membrane hereafter), which can be stretched to a desired pore size within the given recommended range. The top and bottom fluid chambers as well as the qNano membrane were prewetted using the prepared electrolyte buffer. A 75 μL portion of electrolyte buffer was added to the bottom fluid chamber, which was in contact with the *cis* side of the membrane. The qNano membrane was fixed onto the actuating arms of the equipment body and mechanically stretched by adjusting the distance between the arms. Then 40 μL of sample was loaded to the top fluid chamber, which was in contact with the *trans* side of the membrane. The system was allowed to attain a steady baseline current with root-mean-square (rms) noise less than 10 pA for 2 min prior to all data recordings. In between each sample measurement, fresh electrolyte buffer was run at the same voltage and mechanical stretch. A 1.0 kPa transmembrane pressure was applied in the direction of particle flow (*trans* to *cis* side) to fully dislodge any residual particles from the pore. NP70A membranes (detection range 50−150 nm) were used for all experiments.

The voltage applied was optimized to be 0.7 V, at which the trade-off between blockade frequency and background electronic noise was balanced. The size-tunable polyurethane membrane was mechanically actuated to an optimum value of 45 mm. At this stretch value, distinct blockade events were obtained for conjugate groupings while maintaining negligible blockade signal for nAu-DNA probes. These optimized settings were used for all experiments unless stated otherwise.

Data Acquisition. Resistive pulse signals were processed using the Izon Control Suite v2.2 software. A sampling rate of 50 kHz was used. By convention, resistive blockades were detected using the following settings: noise threshold of 8, blockade magnitude of range 0.05−25 nA, and blockade baseline duration of range 0.2 ms to 0.1 s. Noise threshold refers to the minimum ratio of blockade magnitude to rms noise for the signal to be recorded as a successful blockade event. This standard setting was applied for most analyses in this work unless stated otherwise. Raw data, *i.e.*, blockade magnitude, blockade baseline duration, and blockade frequency, were further processed with the software to generate information such as size histogram and scatter plot of blockade baseline duration *versus* blockade magnitude, which were then exported to Microsoft Excel for further processing. To obtain the full signal trace, raw data were exported directly as a .csv file and plotted using Origin software.

Fabrication and Characterization of nAu-DNA Conjugate Grouping. A 1.0 pmol amount of PM target was incubated in a hybridization buffer containing 10 mM PB (pH 7.5), 2.5 mM EDTA, and 100 mM NaCl at 60 °C for 15 min to fully denature all hairpin structures and self-dimers. Approximately 5 nM nAu-100b probe was then incubated with DNA target at 40 °C for 1 h to promote hybridization kinetics. This was followed by the addition of the nAu-18b probe (approximately 15 nM). The final hybridization mixture (volume of 30 μL) was left at room temperature for 20 h to attain hybridization equilibrium. Agarose gel electrophoresis (2% agarose at 5 V/cm, 0.5× TBE as running buffer) was carried out for 120 min at 4 °C to separate the respective order of conjugate groupings formed. Distinct bands corresponding to each order were isolated and left to diffuse into the electrolyte buffer to recover the conjugate groupings.

The respective order of conjugate groupings was loaded separately to the top fluid chamber at a concentration as per gel recovery, quantified to be about 0.1 nM from the UV−vis absorbance value. A different pore stretch and voltage were applied for each order to obtain the optimum signal-to-noise ratio in each case. Blockade events were recorded over 10 min. The size of conjugate groupings was approximated using standard polystyrene particles, which were diluted in the same electrolyte buffer, vortexed gently for 2 min, and sonicated for 10 min prior to use. Standard particles of 70 nm were used to calibrate dimeric and trimeric conjugate groupings, while 118 nm standard particles were used for higher order conjugate groupings.

Real-Time Single-Nucleotide Discrimination. A 40 μL amount of 0.1 nM nAu-18b and nAu-100b probes was loaded into the top fluid chamber of the qNano system. Blockade events for the nAu-DNA probes were recorded over 10 min, which served as a control data set. Then 1.0 pmol of DNA target was added to the top fluid chamber, and data were immediately recorded over the next 30 min in intervals of 10 min. All samples were filtered using a 0.22 μm filter syringe.

Statistical Treatment of Raw Nanopore Data. Each blockade event registered by the nanopore was indicative of one particle translocating through the pore characterized by two key parameters, *i.e.*, blockade magnitude and baseline translocation duration. Each dimension was binned separately using the Freedman−Digconis rule.

$$\text{bin size} = 2\text{IQR}(x)n^{-1/3} \quad (2)$$

where IQR is the interquartile range and n represents the number of data points.

The intersection of bin intervals of the two parameters on the $x-y$ plane defined a grid within which each data point was categorized (Scheme S2). The grid with the highest data density was set as the mode of distribution; 95% of the population, *i.e.*, ±2 SD, centered about the mode, formed the core data set. A similar approach of focusing only on 95% of blockade events for nanopore analysis was previously reported,[40] although the exact method of defining this core data set was not elaborated. All real-time analyses in this paper were carried out on data filtered using this rigorous statistical method.

Conflict of Interest: The authors declare no competing financial interest.

Acknowledgment. This work was supported by research funding from the Singapore Ministry of Education Academic Research Fund Tier 2 *via* grant MOE2008-T2-1-046.

Supporting Information Available: Detailed descriptions of Coulter counting principle, data filtering methodology, DNA probe and target sequences, size distribution of conjugate groupings measured on the nanopore, and an additional TEM micrograph and characterization are provided. This material is available free of charge *via* the Internet at http://pubs.acs.org.

REFERENCES AND NOTES

1. Wang, D. G.; Fan, J.-B.; Siao, C.-J.; Berno, A.; Young, P.; Sapolsky, R.; Ghandour, G.; Perkins, N.; Winchester, E.; Spencer, J.; *et al*. Large-Scale Identification, Mapping, and Genotyping of Single-Nucleotide Polymorphisms in the Human Genome. *Science* **1998**, *280*, 1077–1082.
2. Botstein, D.; Risch, N. Discovering Genotypes Underlying Human Phenotypes: Past Successes for Mendelian Disease, Future Approaches for Complex Disease. *Nat. Genet.* **2003**, *33*, 228–237.
3. Sidransky, D.; Von Eschenbach, A.; Tsai, Y.; Jones, P.; Summerhayes, I.; Marshall, F.; Paul, M.; Green, P.; Hamilton; Frost, P.; *et al*. Identification of p53 Gene Mutations in Bladder Cancers and Urine Samples. *Science* **1991**, *252*, 706–709.
4. Arya, M.; Shergill, I. S.; Williamson, M.; Gommersall, L.; Arya, N.; Patel, H. R. H. Basic Principles of Real-Time Quantitative PCR. *Expert Rev. Mol. Diagn.* **2005**, *5*, 209–219.
5. Li, H.; Huang, J.; Lv, J.; An, H.; Zhang, X.; Zhang, Z.; Fan, C.; Hu, J. Nanoparticle PCR: Nanogold-Assisted PCR with Enhanced Specificity. *Angew. Chem., Int. Ed.* **2005**, *44*, 5100–5103.
6. Erickson, D.; Liu, X.; Venditti, R.; Li, D.; Krull, U. J. Electrokinetically Based Approach for Single-Nucleotide Polymorphism Discrimination Using a Microfluidic Device. *Anal. Chem.* **2005**, *77*, 4000–4007.
7. Baptista, P.; Pereira, E.; Eaton, P.; Doria, G.; Miranda, A.; Gomes, I.; Quaresma, P.; Franco, R. Gold Nanoparticles for the Development of Clinical Diagnosis Methods. *Anal. Bioanal. Chem.* **2008**, *391*, 943–950.
8. Alivisatos, A. P.; Johnsson, K. P.; Peng, X.; Wilson, T. E.; Loweth, C. J.; Bruchez, M. P.; Schultz, P. G. Organization of 'Nanocrystal Molecules' Using DNA. *Nature* **1996**, *382*, 609–611.
9. Mirkin, C. A.; Letsinger, R. L.; Mucic, R. C.; Storhoff, J. J. A DNA-Based Method for Rationally Assembling Nanoparticles into Macroscopic Materials. *Nature* **1996**, *382*, 607–609.
10. Storhoff, J. J.; Elghanian, R.; Mucic, R. C.; Mirkin, C. A.; Letsinger, R. L. One-Pot Colorimetric Differentiation of Polynucleotides with Single Base Imperfections Using Gold Nanoparticle Probes. *J. Am. Chem. Soc.* **1998**, *120*, 1959–1964.
11. Nam, J.-M.; Stoeva, S. I.; Mirkin, C. A. Bio-Bar-Code-Based DNA Detection with PCR-Like Sensitivity. *J. Am. Chem. Soc.* **2004**, *126*, 5932–5933.
12. Storhoff, J. J.; Marla, S. S.; Bao, P.; Hagenow, S.; Mehta, H.; Lucas, A.; Garimella, V.; Patno, T.; Buckingham, W.; Cork, W.; *et al*. Gold Nanoparticle-Based Detection of Genomic DNA Targets on Microarrays Using a Novel Optical Detection System. *Biosens. Bioelectron.* **2004**, *19*, 875–883.
13. Sato, K.; Hosokawa, K.; Maeda, M. Non-Cross-Linking Gold Nanoparticle Aggregation as a Detection Method for Single-Base Substitutions. *Nucleic Acids Res.* **2005**, *33*, e4.
14. Jin, R.; Wu, G.; Li, Z.; Mirkin, C. A.; Schatz, G. C. What Controls the Melting Properties of DNA-Linked Gold Nanoparticle Assemblies? *J. Am. Chem. Soc.* **2003**, *125*, 1643–1654.
15. Zanchet, D.; Micheel, C. M.; Parak, W. J.; Gerion, D.; Alivisatos, A. P. Electrophoretic Isolation of Discrete Au Nanocrystal/DNA Conjugates. *Nano Lett.* **2000**, *1*, 32–35.
16. Qin, W. J.; Yung, L. Y. L. Nanoparticle-Based Detection and Quantification of DNA with Single Nucleotide Polymorphism (SNP) Discrimination Selectivity. *Nucleic Acids Res.* **2007**, *35*, e111.
17. Qin, W. J.; Yung, L. Y. L. Nanoparticle Carrying a Single Probe for Target DNA Detection and Single Nucleotide Discrimination. *Biosens. Bioelectron.* **2009**, *25*, 313–319.
18. Coulter, W. H. *Means for Counting Particles Suspended in a Fluid*. 2656508, 1953.
19. Ito, T.; Sun, L.; Henriquez, R. R.; Crooks, R. M. A Carbon Nanotube-Based Coulter Nanoparticle Counter. *Acc. Chem. Res.* **2004**, *37*, 937–945.
20. Kasianowicz, J. J.; Brandin, E.; Branton, D.; Deamer, D. W. Characterization of Individual Polynucleotide Molecules Using a Membrane Channel. *Proc. Natl. Acad. Sci. U. S. A.* **1996**, *93*, 13770–13773.
21. Fraikin, J.-L.; Teesalu, T.; McKenney, C. M.; Ruoslahti, E.; Cleland, A. N. A High-Throughput Label-Free Nanoparticle Analyser. *Nat. Nanotechnol.* **2011**, *6*, 308–313.
22. Li, J.; Stein, D.; McMullan, C.; Branton, D.; Aziz, M. J.; Golovchenko, J. A. Ion-Beam Sculpting at Nanometre Length Scales. *Nature* **2001**, *412*, 166–169.
23. Ito, T.; Sun, L.; Crooks, R. M. Simultaneous Determination of the Size and Surface Charge of Individual Nanoparticles Using a Carbon Nanotube-Based Coulter Counter. *Anal. Chem.* **2003**, *75*, 2399–2406.
24. Han, A.; Creus, M.; Schurmann, G.; Linder, V.; Ward, T. R.; de Rooij, N. F.; Staufer, U. Label-Free Detection of Single Protein Molecules and Protein−Protein Interactions Using Synthetic Nanopores. *Anal. Chem.* **2008**, *80*, 4651–4658.
25. Saleh, O. A.; Sohn, L. L. Direct Detection of Antibody−Antigen Binding Using an On-Chip Artificial Pore. *Proc. Natl. Acad. Sci. U. S. A.* **2003**, *100*, 820–824.
26. Kowalczyk, S. W.; Kapinos, L.; Blosser, T. R.; Magalhaes, T.; van Nies, P.; LimRoderick, Y. H.; Dekker, C. Single-Molecule Transport across an Individual Biomimetic Nuclear Pore Complex. *Nat. Nanotechnol.* **2011**, *6*, 433–438.
27. Wanunu, M.; Dadosh, T.; Ray, V.; Jin, J.; McReynolds, L.; Drndic, M. Rapid Electronic Detection of Probe-Specific MicroRNAs Using Thin Nanopore Sensors. *Nat. Nanotechnol.* **2010**, *5*, 807–814.
28. Branton, D.; Deamer, D. W.; Marziali, A.; Bayley, H.; Benner, S. A.; Butler, T.; Di Ventra, M.; Garaj, S.; Hibbs, A.; Huang, X.; *et al*. The Potential and Challenges of Nanopore Sequencing. *Nat. Biotechnol.* **2008**, *26*, 1146–1153.
29. Beutler, E. G6PD Deficiency. *Blood* **1994**, *84*, 3613–3636.
30. Wang, Y.; Zheng, D.; Tan, Q.; Wang, M. X.; Gu, L.-Q. Nanopore-Based Detection of Circulating MicroRNAs in Lung Cancer Patients. *Nat. Nanotechnol.* **2011**, *6*, 668–674.
31. Hurley, J. Sizing Particles with a Coulter Counter. *Biophys. J.* **1970**, *10*, 74–79.
32. Yusko, E. C.; Johnson, J. M.; Majd, S.; Prangkio, P.; Rollings, R. C.; Li, J.; Yang, J.; Mayer, M. Controlling Protein Translocation through Nanopores with Bio-Inspired Fluid Walls. *Nat. Nanotechnol.* **2011**, *6*, 253–260.
33. Hill, H. D.; Mirkin, C. A. The Bio-Barcode Assay for the Detection of Protein and Nucleic Acid Targets Using DTT-Induced Ligand Exchange. *Nat. Protoc.* **2006**, *1*, 324–336.
34. Taton, T. A.; Mirkin, C. A.; Letsinger, R. L. Scanometric DNA Array Detection with Nanoparticle Probes. *Science* **2000**, *289*, 1757–1760.
35. Wen, S.; Zeng, T.; Liu, L.; Zhao, K.; Zhao, Y.; Liu, X.; Wu, H.-C. Highly Sensitive and Selective DNA-Based Detection of Mercury(II) with α-Hemolysin Nanopore. *J. Am. Chem. Soc.* **2011**, *133*, 18312–18317.
36. Platt, M.; Willmott, G. R.; Lee, G. U. Resistive Pulse Sensing of Analyte-Induced Multicomponent Rod Aggregation Using Tunable Pores. *Small* **2012**, *8*, 2436–2444.
37. Hayat, M. A. *Colloidal Gold: Principles, Methods, and Applications*; Academic Press: New York, 1989.
38. Phompradit, P.; Kuesap, J.; Chaijaroenkul, W.; Rueangweerayut, R.; Hongkaew, Y.; Yamnuan, R.; Na-Bangchang, K. Prevalence and Distribution of Glucose-6-Phosphate Dehydrogenase (G6PD) Variants in Thai and Burmese Populations in Malaria Endemic Areas of Thailand. *Malaria J.* **2011**, *10*, 368.
39. Qin, W. J.; Yung, L. Y. L. Nanoparticle-DNA Conjugates Bearing a Specific Number of Short DNA Strands by Enzymatic Manipulation of Nanoparticle-Bound DNA. *Langmuir* **2005**, *21*, 11330–11334.
40. Meller, A.; Nivon, L.; Brandin, E.; Golovchenko, J.; Branton, D. Rapid Nanopore Discrimination between Single Polynucleotide Molecules. *Proc. Natl. Acad. Sci. U. S. A.* **2000**, *97*, 1079–1084.